Electronic Supplementary Information (ESI)

Hand-in-hand quantum dot assembly sensitized photocathode for enhanced photoelectrochemical hydrogen evolution

Hao-Lin Wu,[ab] Xu-Bing Li*[ab] Yang Wang,[ab] Shuai Zhou,[ab] Ya-Jing Chen,[ab] Xiao-Jun He,[ab] Chen-Ho Tung[ab] and Li-Zhu Wu*[ab]

[a]Key Laboratory of Photochemical Conversion and Optoelectronic Materials, Technical Institute of Physics and Chemistry, the Chinese Academy of Sciences, Beijing 100190, P.R. China.

[b]School of Future Technology, University of Chinese Academy of Sciences, Beijing 100190, P. R. China.

E-mail: lixubing@mail.ipc.ac.cn; lzwu@mail.ipc.ac.cn.

1. Chemicals

3-Mercaptopropionic acid (MPA, 99%), thioglycollic acid (TGA, 99%), selenium powder (Alfa Aesar, about 200 mesh), Tellurium powder (Alfa Aesar, about 200 mesh), NiO nanoparticles (Alfa Aesar, mean size below 50 nm), $Cd(ClO_4)_2 \cdot 6H_2O$ (99%), $CdCl_2 \cdot 5/2H_2O$ (99%), Na_2SO_3 (99%), $NaBH_4$ (98%) were purchased from Sigma-Aldrich. Other chemicals are of analytical grade without further purification unless otherwise noted. The ultrapure water with 18.2 MΩ cm (Mettler Toledo, FE20, China) was used thorough all experiments.

2. Characterization and Instrument

UV-vis spectra were measured with a Hitachi U-3900 spectrophotometer. Fluorescence measurements were carried out with a Hitachi (model F-4500) spectrophotometer at room temperature. Time-resolved emission decay was measured by time-correlated single photon counting (Edinburgh Instruments, FLS-920) with laser (515 nm) as the excitation light source. The detection limit of the instrument is 0.1 ns. The emission spectra were collected on a PTI instruments spectrofluorimeter equipped with a 75 W Xe-lamp/monochromator excitation source, an R-928 PMT, and single photon counting electronics. All optical measurements were performed at room temperature. TEM images were obtained on a JEM 2100F operating at 200 kV. XPS measurements were taken on an ESCALAB 250 spectrophotometer with Al-Kα radiation. The binding energy scale was calibrated using the C 1s peak at 284.6 eV. Core peaks were analyzed using a nonlinear Shirley-type background. All pH measurements were made with a Model pHS-3C meter (Mettler Toledo FE20, China). Element content was determined by an inductively coupled plasma mass spectroscopy (ICP, Varian710-ES). UV-vis diffuse reflection spectrum was detected with an Agilent Cary 5000 spectrophotometer. The content of oxygen element was measured by Thermo Flash EA 1112 Elemental Analyzer. X-ray absorption spectroscopic (XAS) data were collected at Beam line BL14W1 station of the Shanghai Synchrotron Radiation Facility (SSRF). The storage ring of SSRF was operated at 3.5 GeV with the current of 300 mA. Photoelectrochemistry measurement was carried out in a three-electrode setup with the working electrode of the sample film electrode, counter electrode of platinum disk (5 mm × 20 mm), and reference electrode of Ag/AgCl (3.0 M KCl). An aqueous solution of $Na_4[Fe(CN)_6]$ (1.0 mM) was used to determine the potential of the reference electrode ($E_{Ag/AgCl}$ = +0.194 V *vs.* NHE). The electrolyte (0.1 M Na_2SO_4, pH = 6.8) was degassed for 30 minutes by flushing high purity argon prior to and during each measurement. For photocurrent measurement, the light sources were LED green light (150 mW/cm^2, 520 nm), LED blue light (150 mW/cm^2, 450 nm) or a 300 W Xe-lamp (100 mW/cm^2) with a UV cut-off filter. The light intensity was tested with a Newport photometer. Prior to PEC measurements, the area of the electrode was fixed by insulating cement and the exposed area was 0.36 cm^2. A Zennium electrochemical workstation (Germany, Zahner Company) was used. The transient photocurrent response to on-off illumination was performed when the sample electrode was applied a constant potential (-0.1 V *vs.* NHE). Open circuit potential curve was recorded under on-off illumination. Stability test was performed by chronoamperometry. A constant potential (-0.1 V *vs.* NHE) was applied to the electrode for a period of 4 h while the current density was recorded. The produced hydrogen gas was measured using a gas chromatography (SHIMADZU-GC2014C) equipped with a thermal conductivity detector and a 5 Å molecular sieves GC column. The ultrapure CH_4 was used as internal standard for quantitative analysis.

3. Preparation of Sodium Hydrogen Telluride

The reported method for preparing sodium hydrogen telluride (NaHTe) was used with modification.[1] Briefly, 80 mg of sodium borohydride was transferred to a small flask. Next, 1 mL of ultrapure water was added. After 127.5 mg of tellurium powder was added to the flask, the reaction system was cooled using ice. A small outlet connected to the flask was kept open to discharge the pressure from hydrogen generated during the reaction. Within 3-5 h, the black tellurium powder generally disappeared, and a white sodium tetraborate precipitate appeared on the bottom. The resulting NaHTe in the supernatant was separated to prepare the CdTe particles.

4. Synthesis of Water-Soluble MPA-CdTe QDs

An aqueous colloidal MPA-CdTe QDs solution was prepared using the reaction between Cd^{2+} and NaHTe solutions according to the literature.[1] The Cd^{2+} precursor solution was prepared by mixing solutions of $CdCl_2 \cdot 2.5H_2O$ and stabilizer (MPA) followed by a pH adjustment to 11 with 1.0 M NaOH. The typical molar ratio of Cd:MPA:Te was maintained at 1:1.2:0.2 in our experiment. This solution was placed in a three-necked flask and deaerated with N_2 bubbling, for 30 min. The resulting solution was then heated to 99-100 °C and refluxed for growth of MPA-CdTe QDs with desired size distribution.

5. Synthesis of Water-Soluble TGA-CdSe QDs

An aqueous solution of colloidal TGA-CdSe QDs was synthesized by the reaction between Cd^{2+} and Na_2SeSO_3 according to the method described in our previous work.[2] In details, Cd^{2+} precursor was prepared by mixing a solution of $CdCl_2 \cdot 5/2H_2O$ (46.0 mg, 0.20 mM) and TGA (26 µL, 0.30 mM) in 190 mL ultrapure water. The pH value was then adjusted to 11.0 by 1.0 M NaOH. The solution was deaerated with N_2 bubbling for 30 min, then 10.0 mL freshly prepared

Na_2SeSO_3 solution (5.0 mM) was added into the above solution. Aliquots of the reaction solution were taken out at regular intervals for characterization by UV-vis absorption and emission.

6. General Procedure for the Preparation of CdSe-CdTe QDs assembly

A concentrated solution of 2.0 mL as-prepared TGA-CdSe QDs (2.0×10^{-4} M) was gradually acidification by adding 0.1 M hydrochloric acid until QDs aggregated and then the precipitate was separated by centrifugation (7000 rpm, 6 min) to partially remove the surface bonded stabilizers on CdSe QDs. The obtained precipitate of partial ligand-free CdSe QDs was then redispersed in 2.0 mL ultrapure water and obtained a well-dispersed system via ultrasonic dispersion. Then 50 μL of the above system was added into the 2 mL MPA-CdTe QDs solution (5.0×10^{-6} M) and for a three-minute ultrasonic treatment to obtain a transparent origin stock solution as CdSe-CdTe QDs assembly. The selected centrifugation (i. e., 5000 rpm) was used to remove the unbound CdSe QDs when excessive CdSe aggregates were added to CdTe QDs solution.

7. Photocatalytic H_2 Evolution

Photocatalytic experiments were performed under green LEDs irradiation (150 mW cm^{-2}). The aqueous solution of CdSe-CdTe QDs assembly (5×10^{-6} M) and ascorbic acid (2.84×10^{-2} M, 50 mg/10 mL, pH = 4.65) was degassed by bubbling nitrogen for 30 min before irradiation. Then 600 μL ultrapure CH_4 was injected into the system to work as the internal standard for quantitative GC analysis. The generated molecular H_2 in the reaction headspace was performed by using a gas chromatograph (SHIMADZU-GC2014C) equipped with a thermal conductivity detector and a 5 Å molecular sieves GC column. Argon was used as a carrier gas. The response factor for H_2/CH_4 was about 5.15 under the experimental condition, which was established by calibration with known amounts of H_2 and CH_4, and determined before and after measurements. Error bars on H_2 were calculated from at least three independent experiments. Solar H_2 evolution of bare CdSe QDs and CdTe QDs was performed in a similar procedure.

8. Preparation of NiO Mesoporous Film Electrode

NiO mesoporous film electrode was fabricated following the reported method.[3] In brief, an aqueous suspension of commercially available NiO nanoparticles (mean size below 50 nm) was printed on FTO substrate using a semiautomatic screen printer. FTO substrate with aqueous suspension film of NiO was then sintered at 450 °C for 2.0 hours under air atmosphere, and then the NiO mesoporous film electrode was obtained after being cooled to room temperature.

9. Preparation of the Hand-in-Hand assembly of QD-sensitized Photocathode

The sensitization was realized by subsequent processes of drop casting, air drying and low-temperature calcination under inert atmosphere. Briefly, certain amount of the above-mentioned stock solution of the hand-in-hand assembly of CdSe and CdTe QDs (5.0×10^{-5} M) was dropped on to the surface of NiO film, and the film was dried naturally under ambient condition. Finally, in order to strengthen the binding of QDs on the surface of electrode and avoid the oxidation of QDs, the resulting electrode was calcined in a tube furnace for 20 minutes at 150 °C under Ar(g) atmosphere. The process of low-temperature calcination under inert atmosphere for such a short time can effectively avoid the aggregation and oxidation of QDs, while promoting the surface loading of QDs.[4]

10. Analyzing the number of assemblies on the electrode surface

The number of assemblies on the electrode surface was calculated by following formulas. Firstly, the number of Cd atoms (N) in a single quantum dot can be obtained through formula (1). Among them, V_{QDs} and V_{cell} refer to the volumes of one quantum dot calculated according to the particle size and the unit cell of the quantum dot, respectively. r is the radius of quantum dot, a is the cell parameter, and x is the number of Cd in one cell ($a_{\mathrm{CdSe}} = 6.05 \times 6.05 \times 6.05$; $a_{\mathrm{CdTe}} = 6.26$

× 6.28 × 6.28; X = 4). So, for CdSe and CdTe QDs, the number of Cd atoms is 80 and 184, respectively. Further, the molar mass of the two QDs can be obtained by formula (2) as 10572 g/mol for CdSe and 26551 g/mol for CdTe. Therefore, for an assembly, its mass (m_{assembly}) can be estimated as 6.17 × 10^{-17} mg. Combined with above ICP-OES results, the number of quantum dot assemblies (*N*um) that loaded on per square centimeter of the electrode surface can be calculated as around 3.4 × 10^{15} according to formula (3), where m_{sum} refers to the total mass of the QDs assembly on the surface of the electrode per square centimeter.

$$\mathrm{N}=\frac{\mathrm{V}_{QDs}}{\mathrm{V}_{cell}}=\frac{4\pi \mathrm{r}^3}{3a^3}\times \mathrm{X} \qquad (1)$$

$$\mathrm{M}_r = mA_{r1} + nA_{r2} \qquad (2)$$

$$Num = \frac{m_{sum}}{m_{assembly}} \qquad (3)$$

11. Determine the faradic efficiency of PEC system

The faradic efficiency was determined in a three-electrode system under a bias of -0.1 V vs NHE and blue LEDs irradiation. In a 4.0 h PEC test, total of ~1.10 C charge carriers passed through the external circuit and simultaneously ~5.35 μmol of molecular H_2 was detected by GC for assembly-sensitized electrode system. Herein, the faradic efficiency of PEC H_2 evolution from water splitting was determined to be ~92% by using following equation.

$$\eta_{\text{faradic}} = \frac{2\times n_{H_2}(mol)\times 96485(C/mol)}{Q(C)}\times 100\%$$

in which Q is the total amount of charge passed through the external circuit during the same time period as the measurement of evolved H_2 gas.

12. Analysis of Time-resolved PL Decays of QDs

The excited QDs deactivation was investigated by monitoring the photoluminescence decay as previously reported elsewhere.[5] Multiexponential decay kinetics model can be used to fit the photoluminescence decay to determine the photoluminescence lifetimes for QDs. Then, the average lifetime of QDs photoluminescence decay can be estimated according to the following equation:

$$<\tau>=\frac{\sum_{i=1}^{n}\alpha_i\tau_i^2}{\sum_{i=1}^{n}\alpha_i\tau_i}$$

Where, α_i and τ_i items respectively represent the individual pre-exponential and the lifetime terms, $<\tau>$ represent the average lifetime.

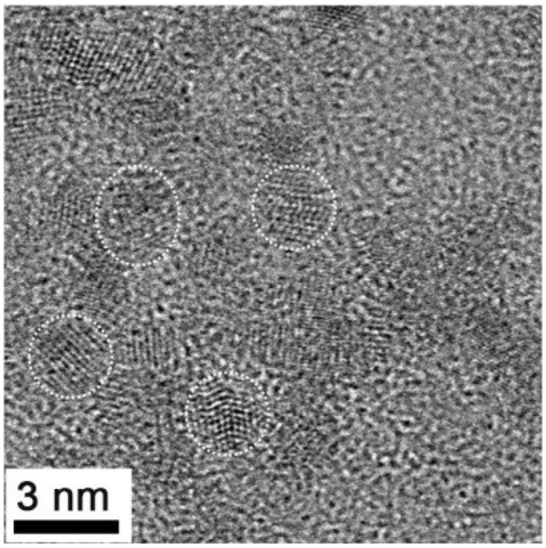

Fig. S1 TEM image of spherical TGA-CdSe QDs, outlined by white circles to give a diameter of ca. 2.0 nm.

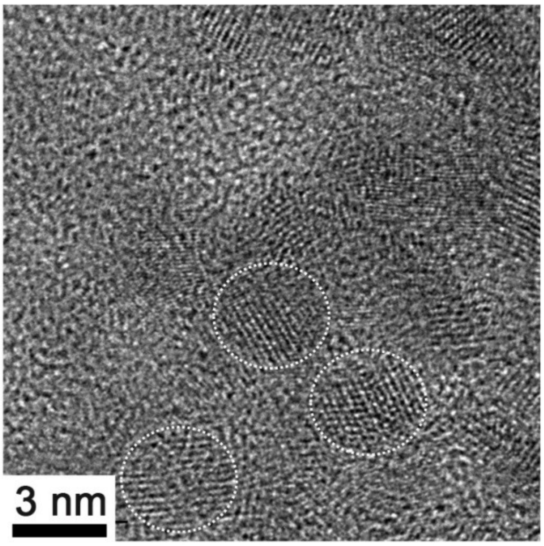

Fig. S2 TEM image of spherical MPA-CdTe QDs outlined by white circles, giving a diameter of *ca.* 2.5 ± 0.5 nm.

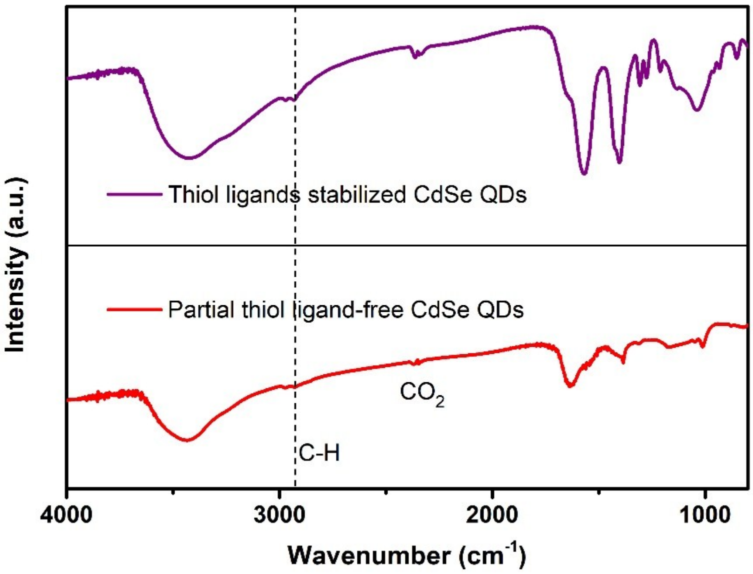

Fig. S3 The Fourier transform infrared spectrum of CdSe QDs before and after the partial removal of surface thiol ligands. After acid treatment, the C-H vibration attributed to thiol compounds decreased significantly, indicating that some of the thiol ligands were removed from the surface of CdSe QDs.

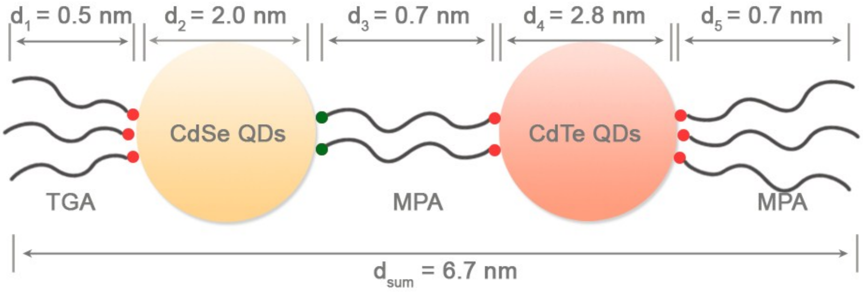

Fig. S4 Schematic illustration of hand-in-hand assembly and the corresponding hydrodynamic size. When assembling the partial ligand-free CdSe QDs with MPA-CdTe QDs through MPA, the size of the resulting assembly is shown as d_{sum}. The length of d_2 and d_4 represents the particle sizes of CdSe QDs and CdTe QDs, which are around 2.0 nm and 2.8 nm, according to the results of TEM images. The d_1 represents the length of TGA, which is around 0.5 nm, on the basis of Gaussian 09 soft. Moreover, according to previous reports, the length of MPA is about 0.7 nm, denoted as d_3 and d_5.[6] Thus the value of d_{sum} can be known as about 6.7 nm, which is close to the results of DLS for the QDs assembly.

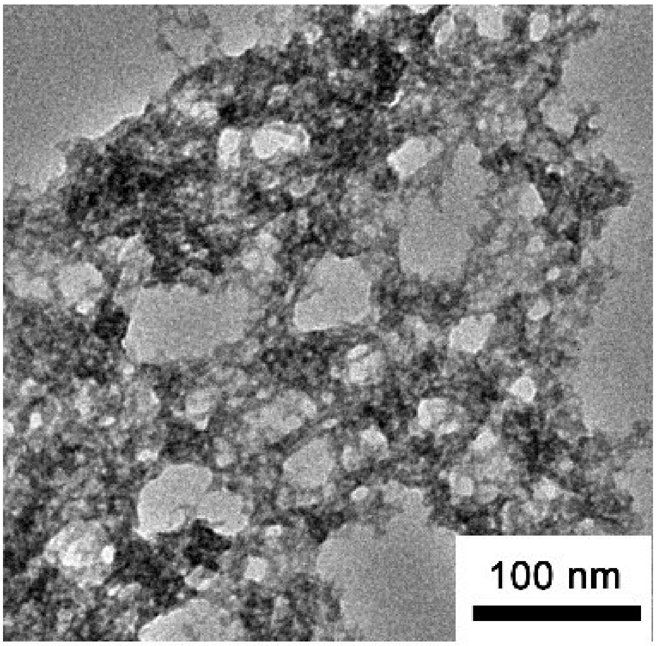

Fig. S5 TEM image of partial ligand-free CdSe QDs, indicating serious aggregation of CdSe nanoparticles before forming hand-in-hand assembly with MPA-CdTe QDs.

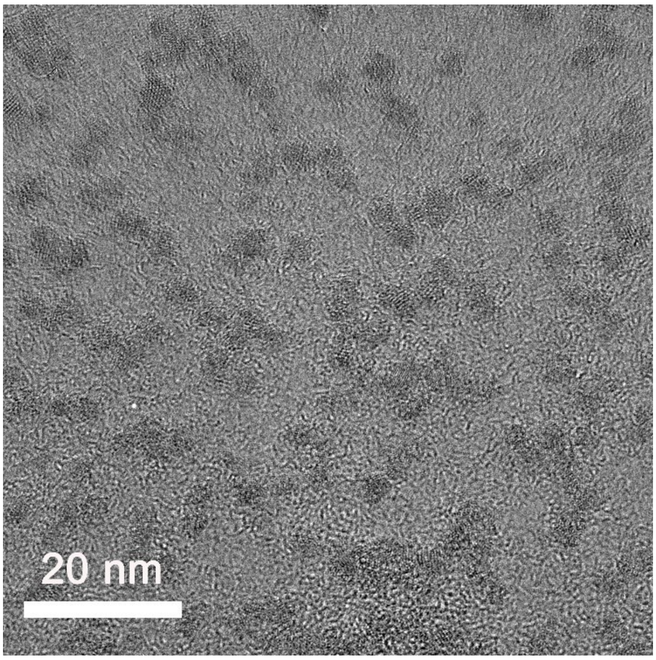

Fig. S6 TEM image of the hand-in-hand assembly of CdSe and CdTe QDs for statistics.

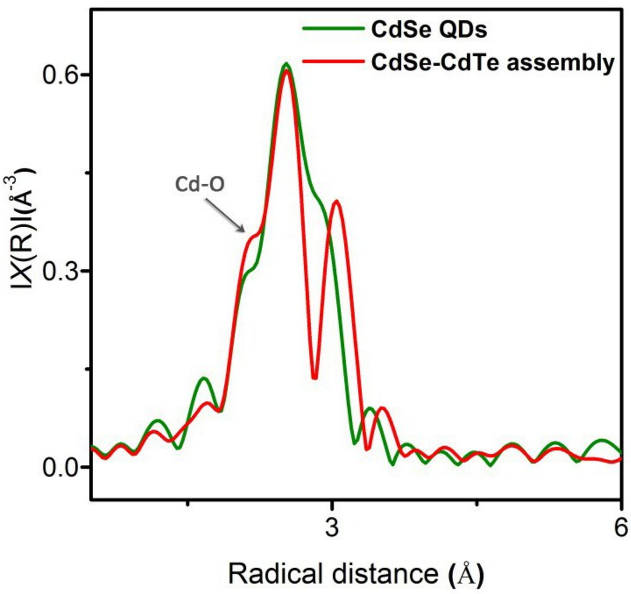

Fig. S7 EXAFS signals of Cd K-edge of partial ligand-free CdSe QDs and the hand-in-hand assembly of CdSe QDs and CdTe QDs in aqueous solution. X-ray absorption spectroscopy (XAS) and measurements were collected by light source at Beam line BL14W1 station of the Shanghai Synchrotron Radiation Research Center (SSRF) at room temperature. The storage ring of SSRF was operated at 3.5 GeV with the current of 300 mA. Energy calibration was performed with a silver foil standard by shifting all spectra to a glitch in the incident intensity. The aqueous solution of CdSe QDs (10^{-4} M) and CdSe-CdTe assembly (10^{-4} M) were encapsulated in the self-sealed bags, respectively. And their fluorescence spectra were recorded using a Lytle fluorescence detector. The obtained data analysis was carried out by Athena software.[7] Firstly, The EXAFS spectra were obtained by subtracting the pre-edge background (-150 to -50 eV *vs.* absorption edge) from the overall absorption and then normalizing with range of 150-700 eV. Subsequently, χ(k) data in the k-space was Fourier transformed to real (R) space using a hanning window (k-weight = 2, k range is from 2.65 to 12.10 Å) to separate the EXAFS contributions from different coordination shells.

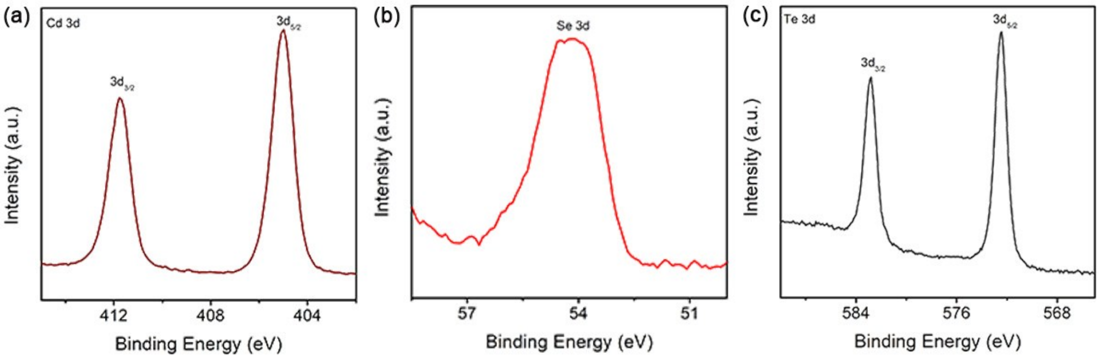

Fig. S8 High-resolution XPS spectra of the hand-in-hand assembly of (a) Cd 3d, (b) Se 3d and (c) Te 3d, respectively.

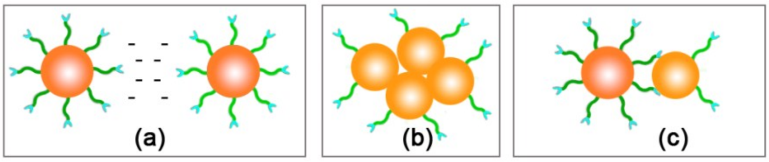

Fig. S9 (a) The electrostatic repulsion between CdTe QDs, (b) aggregation of partial ligands free CdSe QDs, (c) hand-in-hand assembly of CdSe and CdTe.

For MPA-CdTe QDs, the surface of CdTe is tightly coated by the shells of organic ligands of MPA molecules to give them good dispersion in aqueous solutions. Among them, due to the relatively stronger binding constant (~10^9 M^{-1}) between thiol group (-SH) and cadmium atoms, the end of MPA molecule containing -SH can directly bind to the surface of CdTe, while the carboxyl group at the other end is free on the outside of the quantum dot, as shown in Fig. S8a. Based on this situation, the electrostatic repulsion between two negatively charged CdTe QDs makes it difficult to get close to each other, thus inhibiting the formation of CdTe-CdTe assembly. This is also the reason why MPA-CdTe aqueous solution can stably exist for a long time without precipitation. Due to above reason, CdTe-CdTe assembly was not observed in our system. In the case of CdSe QDs, on the other hand, acid treatment causes partial ligands drop off from their surface and expose vacant surface-Cd as well as Se sites. This process makes CdSe QDs metastable since ligands usually act to maintain their water solubility. As a result, CdSe QDs-aggregates can be observed. Obviously, these aggregates composed of multiple QDs is more stable than that of CdSe-CdSe assembly. Therefore, above results suggest that partial absence of surface ligands makes it easier to form aggregates composed of multiple CdSe QDs rather than CdSe-CdSe assembly (Fig. S9b). At this time, when the solution of MPA-CdTe QDs with appropriate concentration is introduced into above system, the ultrasonic process will cause continuous collisions between CdTe and CdSe QDs. According to previous reports, carboxyl group can readily bind at the vacant surface-Cd sites with a binding constant of $\sim 10^6$ M^{-1}. Thus, carboxyl group on MPA ligands of CdTe QDs could spontaneously coordinate on another partial ligand-free CdSe QD at vacant-Cd sites, providing the driving force of hand-in-hand assembly formation (Fig. S9c). Therefore, the probability of assembly between CdSe and CdTe QDs is much higher than that between QDs with the same nature.

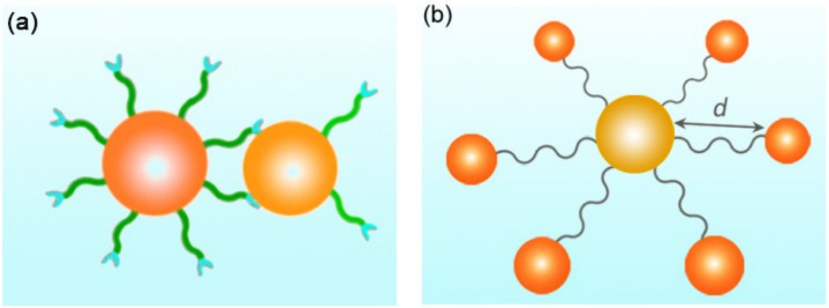

Fig. S10 (a) The hand-in-hand assembly of CdSe and CdTe. (b) The model of multiple-to-one QDs assembly.

Due to the similar sizes of the two QDs (CdTe: 2.8 nm, CdSe: 2.0 nm), assembly of multiple CdSe QDs around a single CdTe has to face significant steric hindrance and vice versa, which is thermodynamically unfavorable. That is to say, the barrier will gradually increase when a second or more CdSe approach the surface of the CdTe, making this less likely to happen. In addition, the short length of MPA is another important factor for the effective control of the assembly composition. Because it also hinders the access and connection of more CdSe since it can be only limited to the vicinity of CdTe. Therefore, it is obvious that in the current system, due to the suitable size of QDs and the length of surface ligands, the majority of CdSe and CdTe QDs were assembled in a 1:1 ratio under ultrasonic.

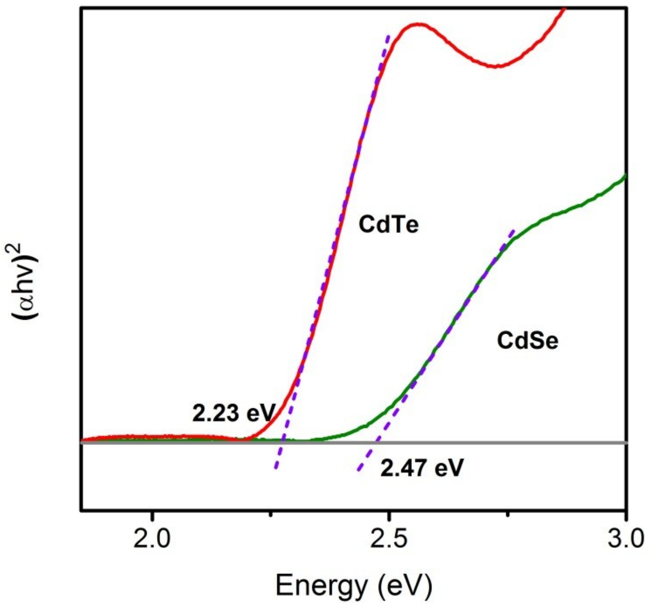

Fig. S11 Tauc Plots of TGA-CdSe QDs and MPA-CdTe QDs, indicating that the band gaps of CdTe and CdSe QDs are 2.23 and 2.47 eV, respectively. Combining with the results of valence-band XPS results of 0.93 and 0.62 V (*vs.* NHE) for CdSe and CdTe QDs, the energy band level of the two kinds of materials can be obtained. The conduction bands level of CdSe and CdTe QDs are -1.62 and -1.54 V *vs.* NHE, respectively. Both the conduction and valence energy levels of CdSe QDs are lower than those of CdTe QDs. Thus, under light irradiation, the photoelectrons will transfer from excited CdTe QDs to CdSe QDs for proton reduction, while photogenerated holes migrate reversely.

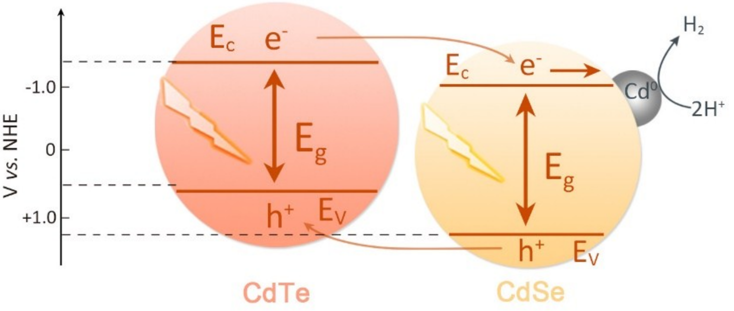

Fig. S12 Type-II band alignment of CdSe QDs and CdTe QDs and the processes of corresponding interparticle charge transfer.

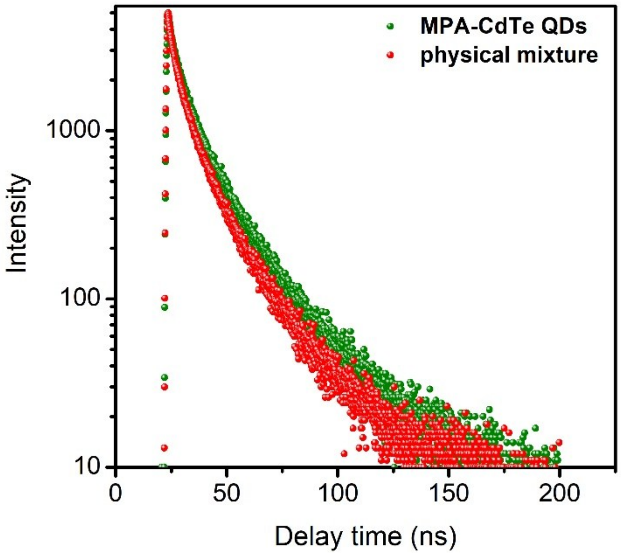

Fig. S13 Time-resolved emission spectra of MPA-CdTe QDs in aqueous solution in the absence and presence of TGA-CdSe QDs. With the existence of CdSe QDs, the average emission lifetime of CdTe QDs decreased from 16.67 ns to 14.43 ns, which is attributing to interparticle electron transfer from excited MPA-CdTe QDs to ground-state TGA-CdSe QDs. MPA-CdTe QDs: 1.0×10^{-5} mol·L^{-1}; light source: 515 nm laser.

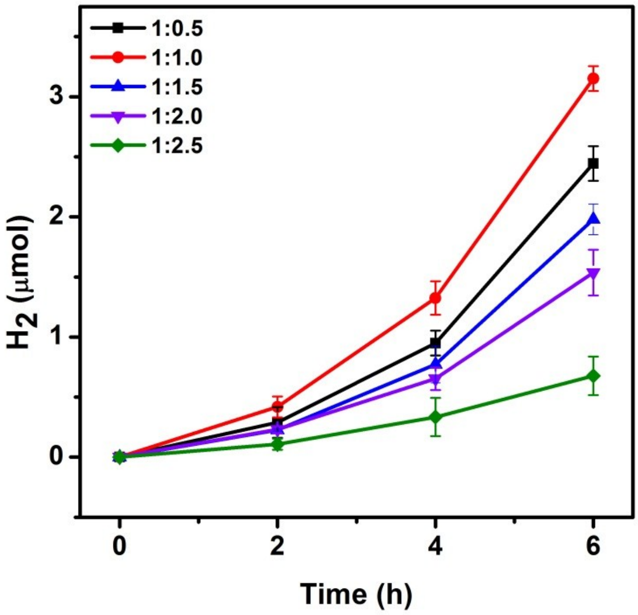

Fig. S14 Photocatalytic H_2 evolution of the nanoparticle assembly with different proportion of CdSe QDs to CdTe QDs. Light source: green LEDs (150 mW cm^{-2}); time: 6 h; electron donor: ascorbic acid (2.84×10^{-2} M, 50 mg/10 mL, pH = 4.65); CdTe QDs: 5.0×10^{-6} mol·L^{-1}; CdSe QDs: increased from 2.5×10^{-6} mol·L^{-1} to 1.25×10^{-5} mol·L^{-1}. Error bars represent mean ±s.d. of at least three independent experiments.

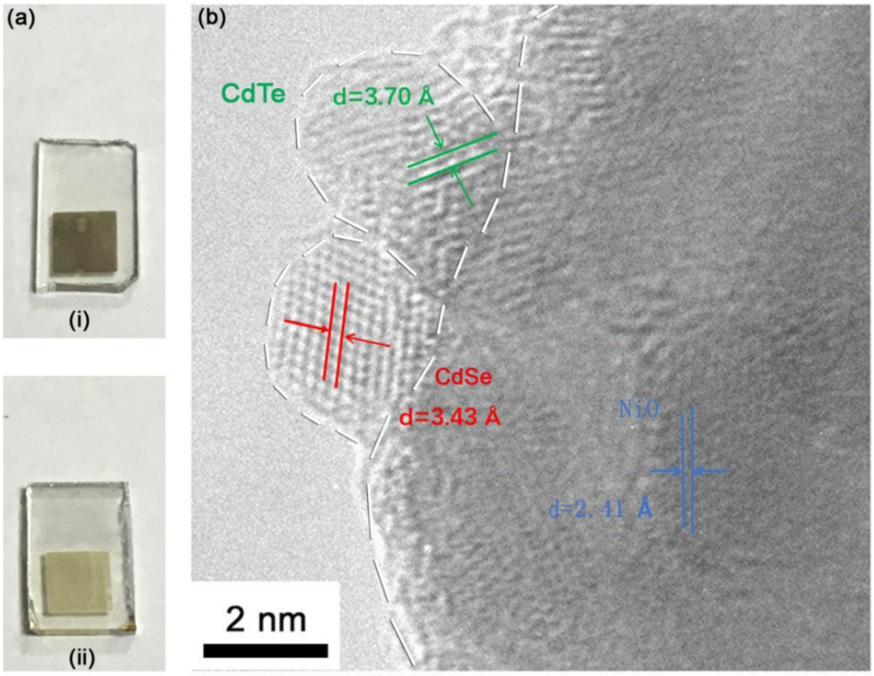

Fig. S15 (a) Photographs of NiO electrode (i) before and (ii) after loading the hand-in-hand assembly of CdSe and CdTe QDs. The change of grey to yellow directly indicates the successful loading of QD-assembly on the surface of NiO electrode. (b) HRTEM image of CdSe-CdTe QDs/NiO, indicating that original sizes of both QDs were well retained on NiO without any mutual aggregation. The lattice spacing of CdSe and CdTe QDs are 3.43 Å and 3.70 Å, respectively.

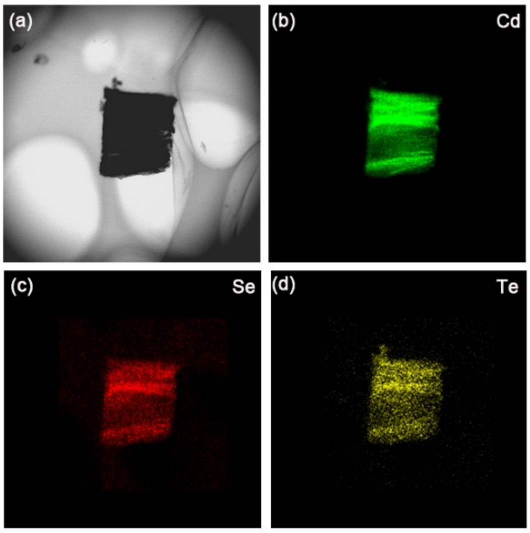

Fig. S16 (a) TEM images of the NiO/CdSe-CdTe film and the corresponding elemental mapping of Cd (b), Se (c) and Te (d) by EDX spectroscopy.

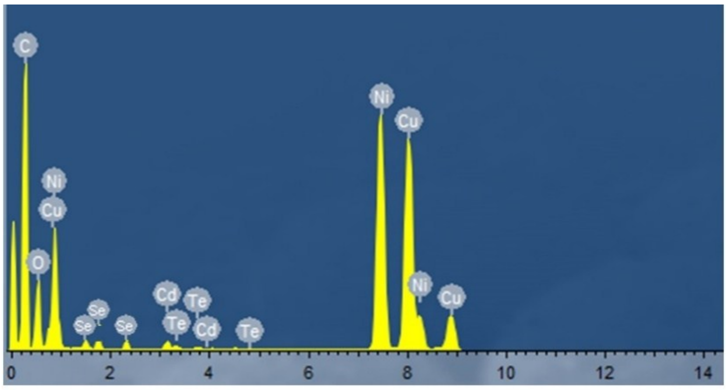

Fig. S17 The overall element spectrum of NiO/CdSe-CdTe film by TEM-EDX spectroscopy.

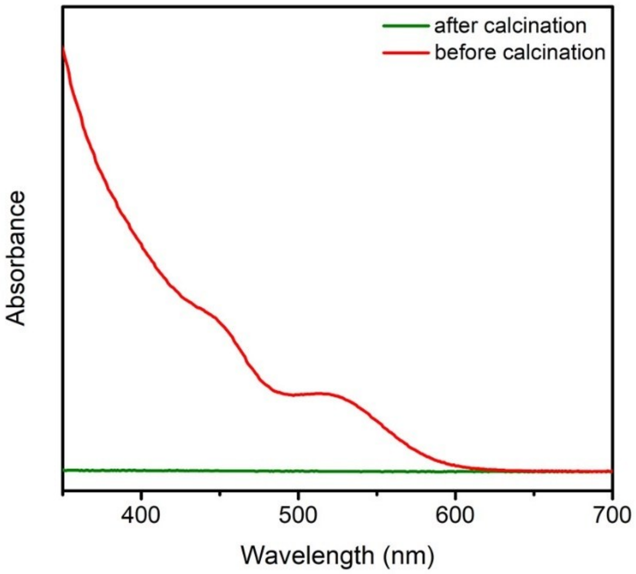

Fig. S18 UV-vis absorption spectra of the aqueous solution with the assembled electrode immersed in solution before and after calcination. If the electrodes coated with the assembly are immersed directly into the aqueous solution without calcination, the assembly will shed significantly from the electrode surface and redissolve in water due to its good water-solubility. At this point, due to the dissolution of QDs assembly, the resulting solution will show obvious characteristic absorption in visible region. The low-temperature curing can promote the interaction between QDs and semiconductor electrodes. When the obtained electrode is immersed in an aqueous solution, no quantum dot shedding can be observed. Correspondingly, no absorption peak appeared in the absorption spectrum of the solution. This experiment shows that the final composition of the electrode can be regulated by controlling the concentration and relative proportion of QDs in the drip-coated solution. Therefore, in our experiment, the 1:1 ratio of the two kinds of QDs on the electrode surface is easy to achieve.

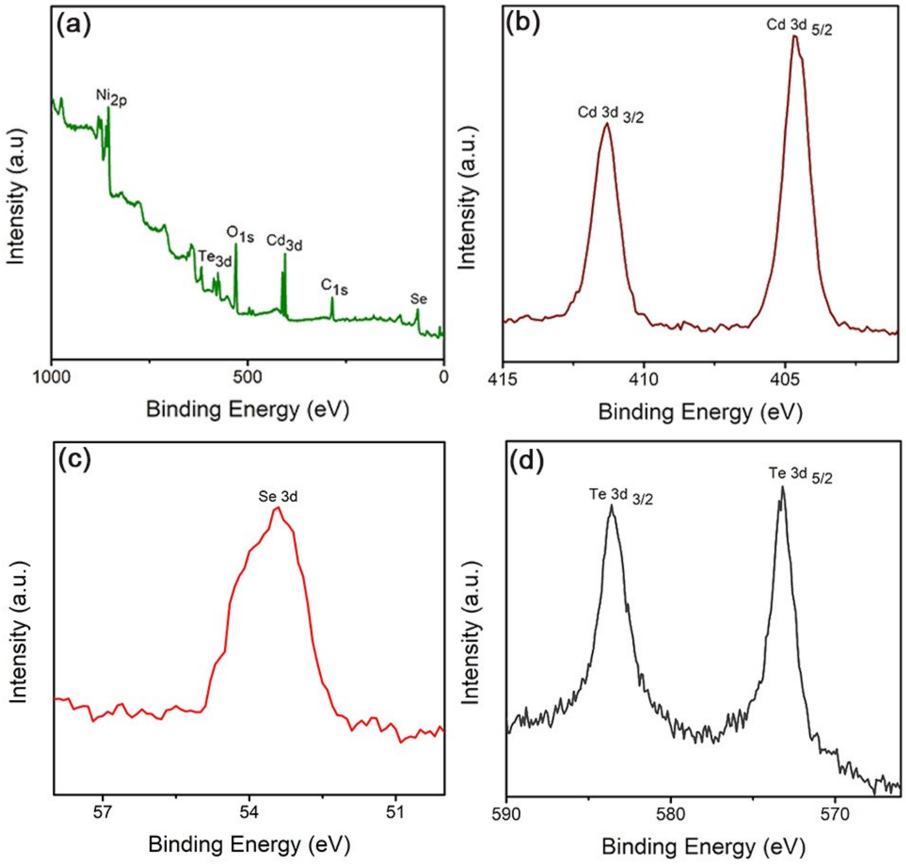

Fig. S19 (a) Full XPS spectrum of the freshly prepared hand-in-hand assembly sensitized NiO electrode and the corresponding enlarged XPS spectra of (b) Cd 3d, (c) Se 3d and (d) Te 3d, respectively.

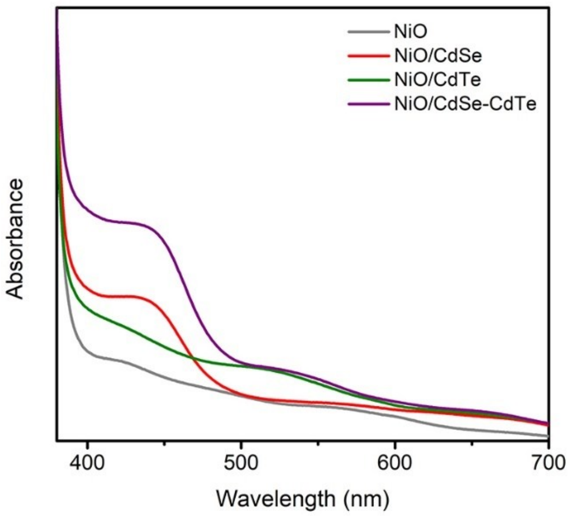

Fig. S20 The UV-vis diffuse reflection spectra of NiO、NiO/CdSe、NiO/CdTe and NiO/CdSe-CdTe electrodes. It can be seen that for the wide-band gap NiO electrode itself, almost no light absorption in the visible region can be observed. The introduction of CdSe or CdTe QDs can extend its absorption to visible region, and the characteristic absorption peak of the corresponding QDs can be observed. It is worth pointing out that, for NiO/CdSe film, there is almost no light absorption intensity above 500 nm, excluding the co-sensitization effect on the PEC performance. That is to say, compared with NiO/CdTe electrode, the improved catalytic performance of the assembled electrode does come from the favorable carrier separation and transport process within the assembly. In addition, the assembly sensitized electrode shows obvious absorption in blue and green region. Therefore, we believe that the enhanced PEC performance detected under blue light conditions is due to the coefficient processes of light absorption and charge separation.

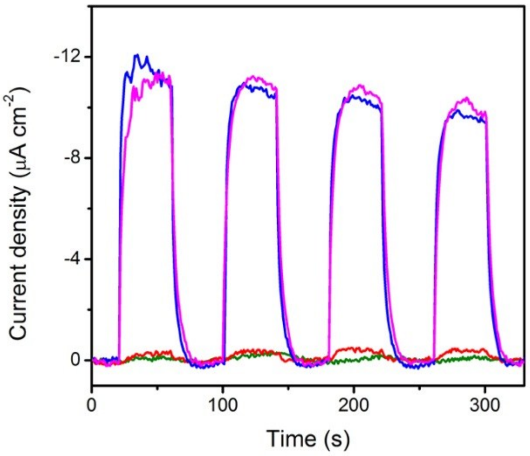

Fig. S21 Transient photocurrent responses to on-off illumination of photocathodes under green light illumination before and after ultrasonic treatment. (red line: CdSe QDs/NiO before ultrasonic; green line: CdSe QDs/NiO after ultrasonic; pink line: CdTe QDs/NiO before ultrasonic; olive line: CdTe QDs/NiO after ultrasonic.) In order to eliminate the possible influence of ultrasonic treatment on the PEC performance of QDs sensitized photocathodes, the solution of CdSe QDs and CdTe QDs was processed by the same ultrasonic method as the process of assembly solution. And the corresponding QDs sensitized photocathodes were tested under identical conditions. It can be seen that ultrasonic treatment has no significant effect on electrode performance.

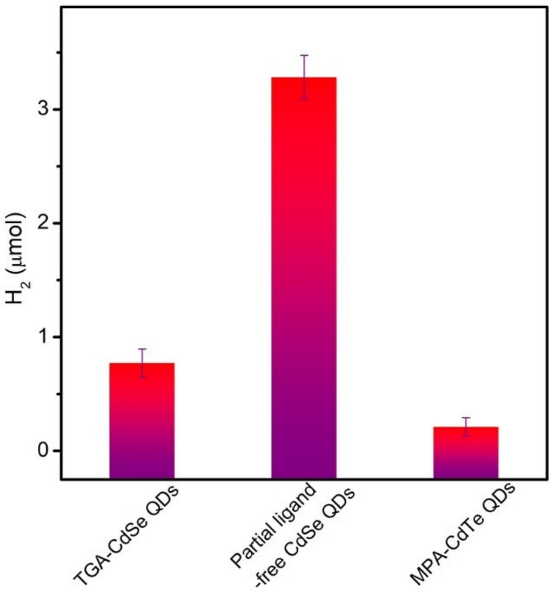

Fig. S22 Photocatalytic H_2 evolution of different QDs-based systems in aqueous solution within two hours under LED blue light illumination. Under the same conditions, the photocatalytic hydrogen production activity of TGA-CdSe QDs before acidic treatment (0.77 μmol) was much lower than those partial ligand-free CdSe QDs (3.28 μmol) within a 2-h measurement. And the photocatalytic hydrogen production activity of CdSe QDs was more than ten times higher than CdTe QDs. Above results show that the assembly design not only improves the efficiency of light absorption and carrier separation, but also enhances the efficiency of surface reaction since photogenerated electrons are used on the surface of more active CdSe QDs.

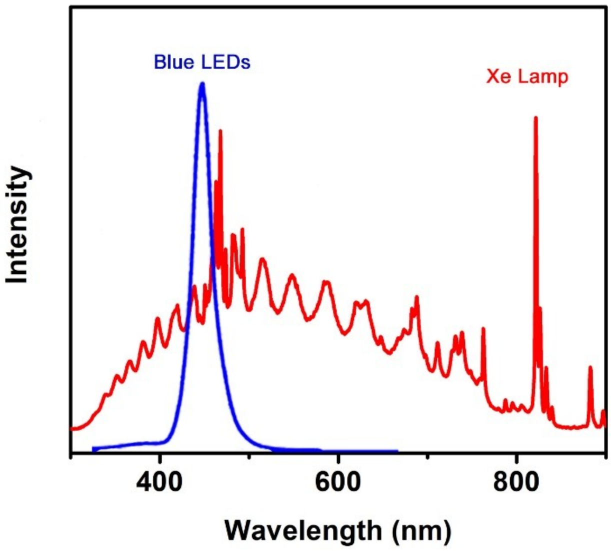

Fig. S23 The spectra of Xe lamp (red line) and blue LEDs (black line) used in our system.

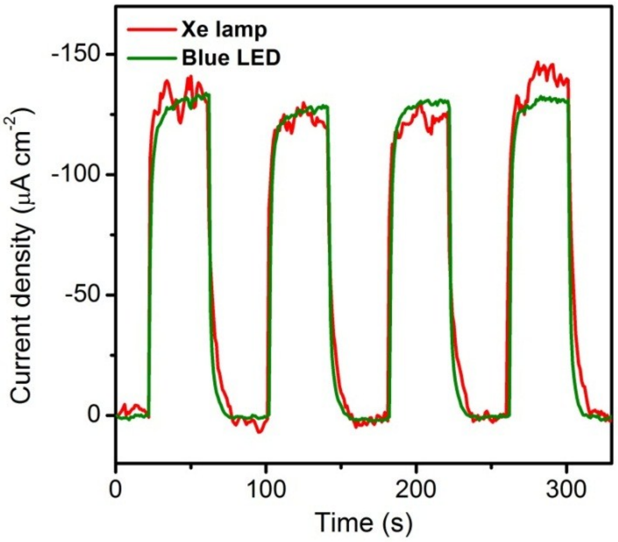

Fig. S24 The transient photocurrent responses to chopped visible-light irradiation with different light sources by taking the hand-in-hand assembly sensitized NiO electrode (~0.36 cm^2) as working electrode, Ag/AgCl (3.0 M KCl) as reference electrode, platinum sheet as counter electrode (5 mm × 20 mm), and 0.1 M Na_2SO_4 as electrolyte, which showed nearly no difference. Xe lamp ($\lambda > 400$ nm): 100 mW cm^{-2}; blue LED: 150 mW cm^{-2}; bias potenbial: -0.1 V *vs.* NHE.

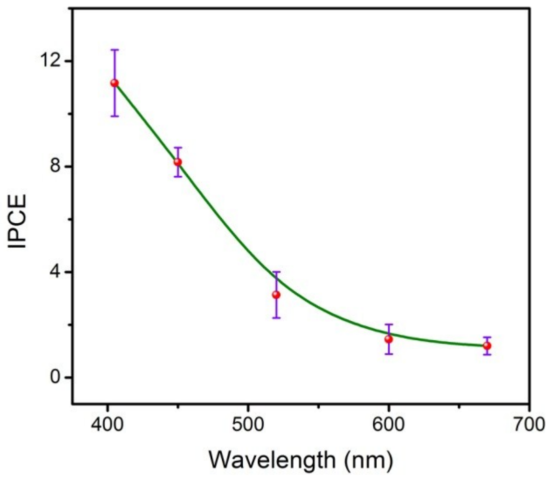

Fig. S25 IPCE spectra of assembly sensitized NiO electrode electrode. Error bars represent mean ± s.d. of three independent experiments.

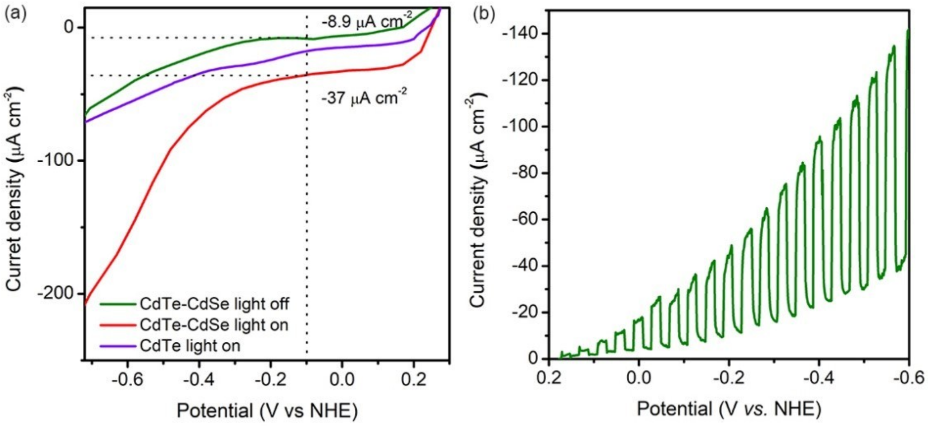

Fig. S26 (a) LSV curves (5.0 mV/s) of CdTe QD/NiO electrode and CdSe-CdTe QD/NiO electrode obtained in the dark and under green light irradiation (150 mW cm^{-2}) and (b) the corresponding chopped LSV curve of CdSe-CdTe QD/NiO electrode by taking the sample photoelectrode (~0.36 cm^{2}) as working electrode, Ag/AgCl (3.0 M KCl) as reference electrode, platinum sheet as counter electrode (5 mm × 20 mm), and 0.1 M Na_2SO_4 as electrolyte.

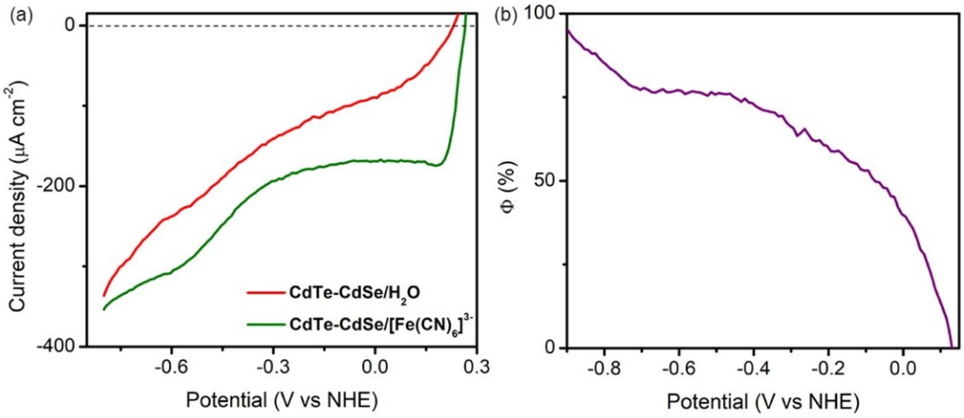

Fig. S27 (a) J-V curves of the photocathode with and without [Fe (CN)$_6$]$^{3-}$ anions in electrolyte. (b) Charge separation and injection efficiency (Φ)of the photocathode. Electrolyte: 0.1 M Na_2SO_4 (pH = 6.8) + 2.5 mM $K_3[Fe(CN)_6]$.

For CdSe-CdTe QDs assembly, when used in aqueous solution for photocatalytic hydrogen production, ascorbic acid was used as the sacrificial reagent to consume redundant photoholes. When the assembly is loaded on the electrode surface, the system was able to achieve stable hydrogen production in neutral aqueous solutions without any sacrificial reagents. Photoelectrons participate in H_2 evolution while photogenerated holes migrate to the anode for water oxidation. In this case, if sacrificial electron acceptor such as [Fe(CN)$_6$]$^{3-}$ anions are added into the system, they will compete with hydrogen production to scavenge the photogenerated electrons that arrive at the electrode/solution interface. Since the more advantages in thermodynamics, electrons that reach the electrode's surface preferentially react with [Fe(CN)$_6$]$^{3-}$ anions, and almost no hydrogen is produced. Therefore, a charge separation and injection efficiency higher than 50% can be obtained with a bias potential lower than -0.2 V vs NHE (Fig. S27b). Similarly, if sacrificial electron donors are introduced (e.g., Na_2S), they will be oxidized at the anode instead of water oxidation.

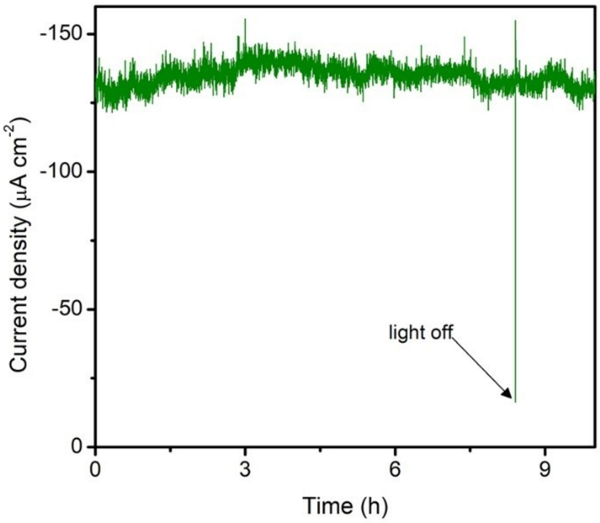

Fig. S28 Ten-hour stability measurement of the PEC system with NiO/CdSe-CdTe assembly as the photocathode.

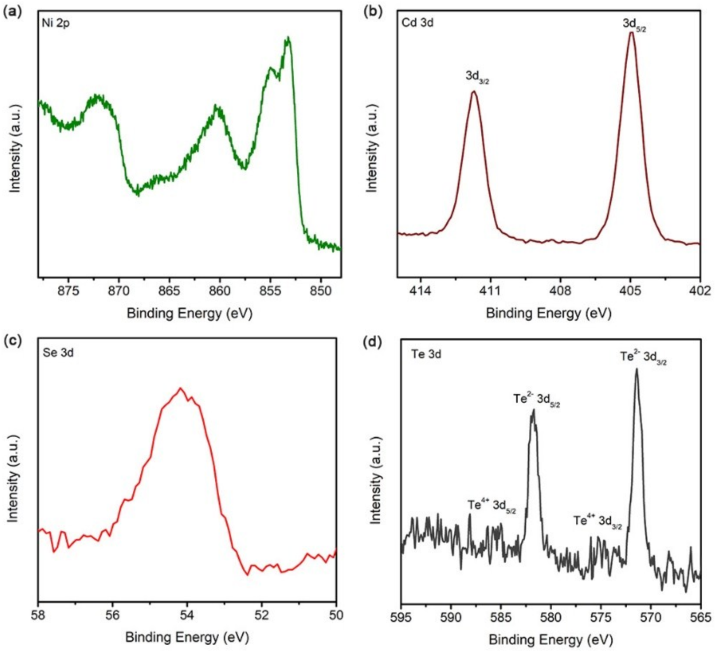

Fig. S29 High-resolution XPS spectra of the hand-in-hand assembly sensitized NiO electrode after a 10-h PEC measurement of (a) Ni 2p, (b) Cd 3d, (c) Se 3d and (d) Te 3d, respectively.

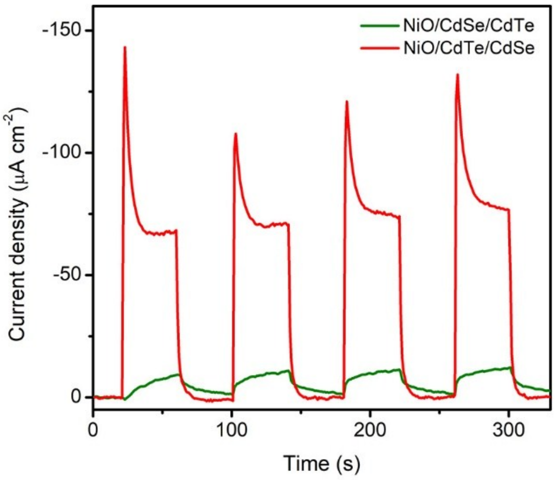

Fig. S30 Transient photocurrent responses to on-off illumination of photocathodes made by layer-by-layer methods (red line: NiO/CdTe/CdSe; green line: NiO/CdSe/CdTe).

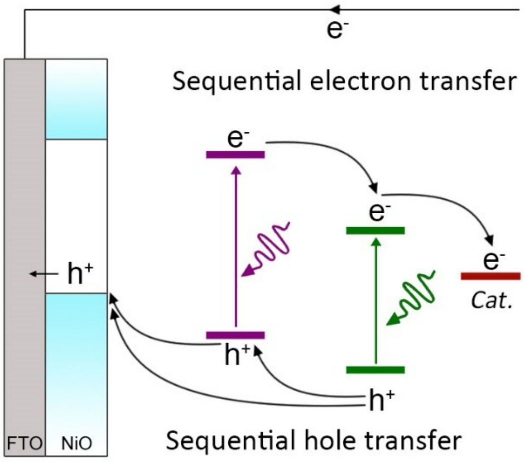

Fig. S31 The illustration of sequential charge transfer at electrode interfaces and the corresponding band alignment.

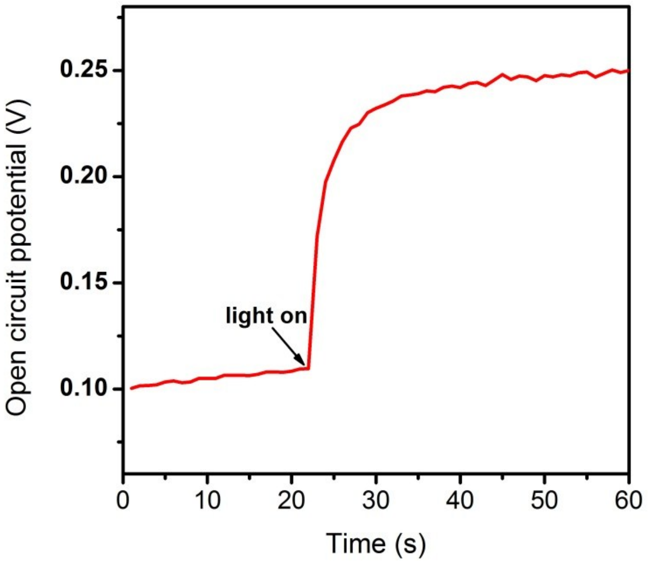

Fig. S32 Open circuit potential (OCP) responses under LED green light illumination for the hand-in-hand assembly of CdSe and CdTe QDs sensitized NiO photocathode. Under green light irradiation, a positive photo-voltage of around 150 mV can be observed, which means the process of hole injection into the surface of the NiO film. The sample photoelectrode (~0.36 cm^2) was used as working electrode, Ag/AgCl (3.0 M KCl) was reference electrode, platinum sheet was counter electrode (5 mm × 20 mm), and 0.1 M Na_2SO_4 was the electrolyte.

Table S1. Oxygen content of different QDs samples measured by Elemental Analyzer.

Sample	**TGA-CdSe**	**partial ligand-free CdSe**	**MPA-CdTe**	**CdSe-CdTe assembly**
Content (%)	2.86%	2.37%	3.35%	2.74%

It can be seen that for the freshly prepared TGA-CdSe QDs, the content of oxygen element is about 2.86%, which may mainly come from the presence of carboxyl ligands ($-COO^-$) containing oxygen on the surface of QDs. When the ligands are partially removed, the oxygen element content is equal to 2.37%, meaning that the acid treatment does not cause drastic changes of CdSe QDs. Accordingly, the content of oxygen in the assembly after ultrasonic treatment is about 2.74%. These results suggest that the assembly process did not significantly lead to the oxidation of the surface of QDs. Therefore, the significantly enhanced signal at 2.2 Å in EXAFS should not come from the CdSe and/or CdTe surface oxidation to CdO.

Table S2. Transient lifetime obtained from the signal monitored at 550 nm.

Entry	*τ_1 (ns)*	*B_1*	*τ_2 (ns)*	*B_2*	*τ_3 (ns)*	*B_3*	*$\tau_{average}$ (ns)*	*Rate of ET*
MPA-CdTe QDs[a]	2.54	1886.8	10.5	2370.9	28.8	632.5	16.6	9.0×10^6 s^{-1}
Physical mixture of MPA-CdTe and TGA-CdSe QDs[a]	2.37	2044.3	9.56	2276.0	27.3	465.7	14.43	
MPA-CdTe QDs[b]	0.142	0.269	2.42	0.018	16.2	0.003	7.72	6.8×10^7 s^{-1}
CdSe-CdTe assembly[b]	0.233	0.186	2.35	0.014	15.0	0.002	5.06	

[a]The time-resolved emission measurements were carried out in aqueous solution. When adding TGA-CdSe QDs in to the solution of MPA-CdTe QDs, the resulting physical mixture showed a shorter lifetime, from 16.6 ns to 14.43 ns. [b]The time-resolved emission measurements were carried out on the surface of insulating SiO_2 to exclude the influence of hole transfer. Compared with the solid of MPA-CdTe QDs, the CdSe-CdTe assembly on the surface showed a shorter lifetime of 5.06 ns, which means the existence of efficient electron transfer within the assembly. According to the calculated rates (9.0×10^6 s^{-1} for physical mixture and 6.8×10^7 s^{-1} for assembly) of interparticle electron transfer, it can be found that the formation of nanoparticle assembly greatly facilitates the process of interparticle electron transfer.

Table S3. TEM-EDX element analysis of QDs assembly on the electrode surface.

Element	Weight percentage (wt%)	atomic ratio (At%)
Cd	1.79	3.72
Se	0.12	0.35
Te	0.26	0.46

Table S4. Element concentration (Mean±SD μg/g) in diluted solution obtained by ICP-OES (*n*=3) of the freshly prepared NiO/assembly electrode.

Sample	**Cd**	**Se**	**Te**
Concentration (Mean±SD μg/g)	15.12±0.16	1.58±0.07	2.06±0.11

To judge about the QDs density on the NiO surface, the content of QDs assembly on the electrode surface was firstly investigated by the ICP-OES measurement. The specific experimental details are as follows. Firstly, the assembly electrode with a certain surface area is dissolved by certain volume of aqua regia. After sufficiently diluted, the content of QDs in the trial solution can be calculated by comparing the experimental results with the standard curves of Cd, Se and Te elements. After that, the concentration of QDs dissolved in the original solution (μg/g) can be obtained according to the known dilution ratio and the corresponding solution weight. Finally, the amount of assembly loaded per square centimeter is obtained according to the known electrode area. The results are the average values of multiple collections.

Table S5. Summary of the reported QD-sensitized photocathodes for PEC H_2 evolution.

Photocathode	**Electrolyte/pH**	**Bias**	**Current density**	**Reference**
Au/InP QDs/ [$Fe_2S_2(CO)_6$]	0.1 M $NaBF_4$ pH 7 solution	-0.4 V *vs.* Ag/AgCl	-100 nA cm^{-2}	*Angew. Chem. Int. Ed.* **2010**, *49*, 1574
Au/P3HT/CdSe QDs/Pt	0.1 M phosphate pH 7 buffer solution	-0 V *vs.* RHE	-1.2 mA cm^{-2}	*ACS Appl. Mater. Inter.* **2015**, *7*, 19083
p-Si/ InP QDs/[$Fe_2S_2(CO)_6$]	0.1 M H_2SO_4	-0.5 V *vs.* Ag/AgCl	-1.2 mA cm^{-2}	*J. Mater. Chem. A* **2014**, *2*, 9478
NiO/CdSe QDs/NiS	0.5 M Na_2SO_4 pH 6.8 solution	0 V *vs.* Ag/AgCl	-130 μA cm^{-2}	*ACS Nano* **2014**, *8*, 10403
NiO/CdSe QDs/[$Co(bdt)_2$]$^-$	0.1 M KCl pH 7 solution	-0.28 V *vs.* RHE	-2 mA cm^{-2}	*ACS Catal.* **2015**, *5*, 2255
NiO/CdSe QDs	0.1 M Na_2SO_4 pH 6.8 solution	-0.1 V *vs.* NHE	-60 μA cm^{-2}	*Energ. Environ. Sci.* **2015**, *8*, 1443
NiO/CdSe QDs/CoHEC	0.1 M Na_2SO_4 pH 6.8 solution	0 V *vs.* NHE	-110 μA cm^{-2}	*J. Mater. Chem. A* **2015**, *3*, 18852
Au/SWCNT/InP/ZnS QDs	0.1 M phosphate pH 7 buffer solution	0 V *vs.* Ag/AgCl	-0.7 μA cm^{-2}	*J. Mater. Chem. C* **2016**, *4*, 3379
Cu_2S/C QDs	1 M KCl pH 5.97 solution	0 V *vs.* NHE	-1.05 mA cm^{-2}	*Nanoscale* **2016**, *8*, 8559
NiO/CdTe QDs/NiS	0.1 M phosphate pH 6 buffer solution	-0.222 V *vs.* Ag/AgCl	- 40 μA cm^{-2}	*ACS Appl. Mater. Inter.* **2015**, *3*, 2429
NiO/CdSe QDs	0.1 M phosphate pH 6.8 buffer solution	0 V *vs.* RHE	-20 μA cm^{-2}	*Phys. Status Solidi A* **2014**, *211*, 1868
NiO/CdSe QDs /MoS_2	a buffer solution (pH 6) containing 0.3 M $C_6H_{12}N_4$), 0.1 M HCl, and 0.2 M KCl	-0.131 V *vs.* RHE	-60 μA cm^{-2}	*Chem-Asian J.* **2015**, *10*, 1660
NiO/PTZ/CdSe QDs	0.1 M Na_2SO_4 solution	-0.1 V *vs.* NHE	-180 μA cm^{-2}	*Adv. Sci.* **2016**, *3*, 1500282
GDY/CdSe QDs	0.1 M Na_2SO_4 solution	0 V *vs.* NHE	-70 μA cm^{-2}	*J. Am. Chem. Soc.* **2016**, *138*, 3954
NiO/CdSe QDs/CoHEC	0.2 M HMTA/HCl pH 6 buffer solution with 0.1 M KCl	0 V *vs.* Ag/AgCl	-115 μA cm^{-2}	*P. Natl. Acad. Sci. USA* **2017**, *114*, 11297
NiO/MAA/CdSe QDs	0.1 M Na_2SO_4 pH 6.8 solution	-0.1 V *vs.* NHE	-136 μA cm^{-2}	*Part. Part. Syst. Char.* **2017**, 1700278

Table S6. Element concentration (Mean±SD μg/g) in diluted solution obtained by ICP-OES (*n*=3) of NiO/assembly electrode after the 10-h PEC measurement.

Sample	**Cd**	**Se**	**Te**
Concentration (Mean±SD μg/g)	14.21±0.09	1.50±0.10	1.85±0.08

After a 10-hour PEC measurement, a slight decrease of QDs content on electrode can be detected (from ~0.21 mg/cm^{-2} to ~0.19 mg/cm^{-2}), which indicates the slight shedding of some QDs in the experiment. However, the ratio of two kinds of QDs on the electrode surface showed faint changes and the ratio is still close to 1:1, suggesting that the electrode structure is relatively stable.

Reference

1. H. Zhang, Z. Zhou, B. Yang and M. Gao, *J. Phys. Chem. B,* 2002, **107**, 8.
2. Z. J. Li, J. J. Wang, X. B. Li, X. B. Fan, Q. Y. Meng, K. Feng, B. Chen, C.-H. Tung and L.-Z. Wu, *Adv. Mater*., 2013, **25**, 6613.
3. A. Nattestad, A. J. Mozer, M. K. R. Fischer, Y. B. Cheng, A. Mishra, P. Bauerle and U. Bach, *Nat. Mater.,* 2010, **9**, 31.
4. L. P. Liu, J. Hensel, R. C. Fitzmorris, Y. D. Li and J. Z. Zhang, *J. Phys. Chem. Lett.,* 2010, **1**, 155.
5. A. Kongkanand, K. Tvrdy, K. Takechi, M. Kuno and P. V. Kamat, *J. Am. Chem. Soc*., 2008, **130**, 4007.
6. V. L. Colvin, A. N. Goldstein and A. P. Alivisatos, *J. Am. Chem. Soc*., 1992, **114**, 5221.
7. B. Ravel and M. Newville, *J. Synchrotron Rad.,* 2005, **12**, 537-541.